Computational Materials Science 192 (2021) 110380

Contents lists available at ScienceDirect

Computational Materials Science

journal homepage: www.elsevier.com/locate/commatsci

Electronic charge density as a fast approach for predicting Li-ion migration pathways in superionic conductors with first-principles level precision

Yinqiao Liu [a,b], Xue Jiang [a,*], Jijun Zhao [a], Ming Hu [b,*]

[a] Key Laboratory of Materials Modification by Laser, Ion and Electron Beams (Dalian University of Technology), Ministry of Education, Dalian 116024, China
[b] Department of Mechanical Engineering, University of South Carolina, Columbia, SC 29208, USA

ARTICLE INFO

Keywords:
Ionic Conductivity
First-principles
Migration Pathways
Electronic Charge Density
Material Descriptor

ABSTRACT

Finding Li-ion migration pathways in solid state electrolytes is an important prerequisite for disruptive development of all-solid-state battery materials. Previous studies either used empirical method such as bond valence (BV) or relied on on-the-fly first-principles molecular dynamics (FPMD) simulations, which are very time and resource consuming. In this paper, we propose an approach of using spatially dependent electronic charge density to predict Li-ion migration pathways in superionic conductors with first-principles level precision. Since the electronic charge density can be simultaneously calculated along with the structure optimization, this method saves tremendous computing time in finding the migration pathways, as is the case for the currently widely used FPMD method. Its accuracy and feasibility are validated by reproducing 3D diffusion channel of six representative Li-ion structures [$LiFePO_4$, Li_2S, $Li_5PS_4Cl_2$, $Li_{10}GeP_2S_{12}$, Li_4GeS_4, and $Li_3Y(PS_4)_2$]. Our approach is expected to accelerate high-throughput screening of superionic conductors, such as using the most likely migration paths replaces global search of migration paths for first-principles method. The direct relationship between ion transport pathways and electronic charge densities constructed here could serve as an efficient descriptor for training machine learning models. Due to the inherent relationship between bottom-level electronic charge density and macroscopic properties, we expect that this method can be also extended to designing materials with other target physical or chemical properties such as thermoelectrics, photovoltaics, and fuel cells.

1. Introduction

Lithium ion batteries (LIBs) have become instrumental in powering nearly all of our small, portable electronics and are also of great interest for grid-scale energy storage, due to their large specific capacity, long storage, cycle life, and environmental friendliness [1–3]. However, all-solid-state lithium-ion batteries (ASSLIBs) [4] are promising next generation LIBs for energy storage that holds the promise to be both more energy dense as well as safer [5] than traditional organic-liquid-electrolyte-based batteries. High performance electrolytes require high lithium ionic conductivity (σ) and connected lithium ion pathways, which can be measured directly by neutron diffraction in experiment [6,7]. Theoretically, Li ionic conductivity and migration pathways can be acquired by atomistic simulations [8–10]. However, such calculations can be either very expensive, e.g. empirical or first-principles molecular dynamics (FPMD) simulation, or require prior knowledge for the transition paths, e.g. the nudged elastic band (NEB) method coupled with first-principles calculation. Because of these difficulties, involving too much FPMD simulations to directly calculate the ionic conductivity is too computationally expensive and is not realistic for future large-scale screening and optimization of Li-battery materials.

Nevertheless, pioneering work on screening fast ionic conductors has been conducted in recent years. Wang et al. highlighted the importance of bcc-like anion framework desirable for achieving high ionic conductivity in several known fast ion conductors [11], which pointed out a clear direction for the design of superionic conductors. Ong group recently developed a tiered screening strategy that combines topological analysis with FPMD simulations to rapidly exclude bad or poor candidates [12], with example of Li-P-S and Li-M-P-S families. The bond valence (BV) method [13] has become particularly appropriate and promising for this screening task. The BV approach enables the fast construction of bond valence energy landscapes (BVELs) and therefore direct exploration of ion migration pathways. Recently, Chen et al. combined the BV theory and the Ewald summation to improve over the original BV model by including the Li-cation repulsion [14]. Katcho et al. first reported the technical details of the automation of the BV

* Corresponding authors.
E-mail addresses: jiangx@dlut.edu.cn (X. Jiang), hu@sc.edu (M. Hu).

https://doi.org/10.1016/j.commatsci.2021.110380
Received 28 November 2020; Received in revised form 4 January 2021; Accepted 8 February 2021

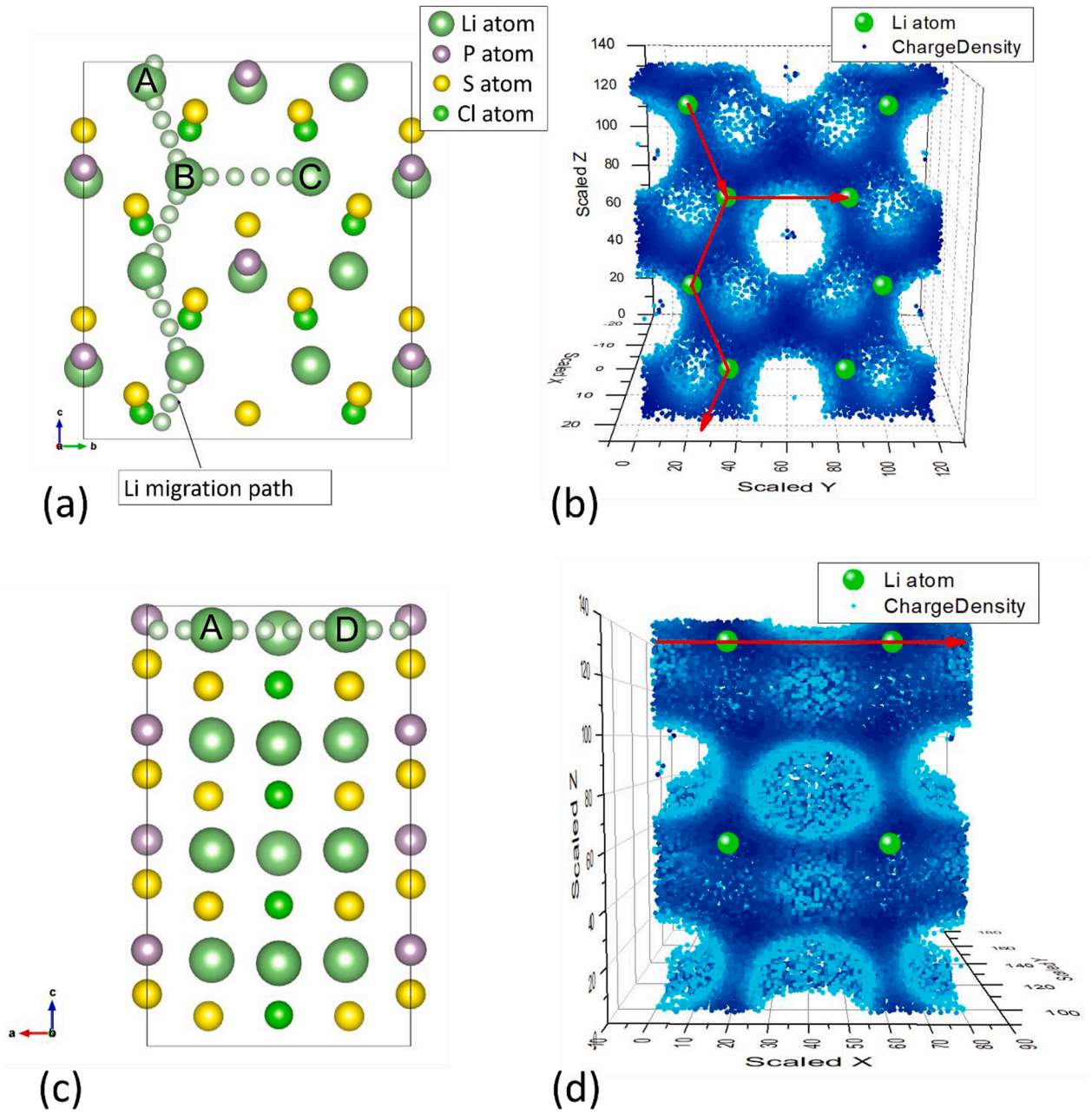

Fig. 1. Li ion transport in $Li_5PS_4Cl_2$. (a), (c): Schematic of 3D Li ion diffusion channel (light green balls) [12]. (b), (d): 3D spatial electronic charge density distribution in a section along *c*-axis, *b*-axis, and along the *a*-axis of the $Li_5PS_4Cl_2$, respectively. The lithium ions are shown by the green balls. The dark blue region represents the possible Li ion diffusion channel. The red arrows indicate the migration channels from the left panel.

calculations and additionally they used machine learning to evaluate the predictive capabilities of the structural descriptors. Although BV theory can generate a lot of data in a short time, the method is in principle based on classical force field [15,16]. Thus, the quality of the prediction is questionable, and the final target value of ionic conductivity was not predicted.

In short, the existing high-throughput screening of Li-containing fast ionic conductors generally resort to the intensive use of FPMD simulations, which inevitably brings significant computational burden, while fast evaluation of the dominant factors through fully static but relatively faster first-principles calculations receives less attention. Previous machine learning studies and high-throughput screening either intensively used the elemental and structural descriptors with small training dataset or only focused on specific structures or families, and thus the trained models may not converge well and lack the general application as well. Therefore, we propose to conduct fully static first-principles calculations for screening the lithium ionic conductors by evaluating the ion migration pathways and associated activation energy. We introduce a new and effective descriptor – spatially dependent electronic charge density – to establish a mapping between easily accessible attributes of a system and diffusion barrier energy. The enormously low computational cost of the electronic charge density calculation will dramatically speed up the structure screening while maintaining high precision of first-principles calculations, compared with direct FPMD simulations and BV method. In the following, we will first calculate the electronic charge density of 4 known complex structures [$Li_5PS_4Cl_2$, $Li_{10}GeP_2S_{12}$, Li_4GeS_4 and $Li_3Y(PS_4)_2$] with high ionic conductivity and one simple structure (Li_2S), and then perform topological analysis to identify the 3D transport channels. We will then demonstrate that the electronic charge density is an effective approach to find the ion transport pathways in different

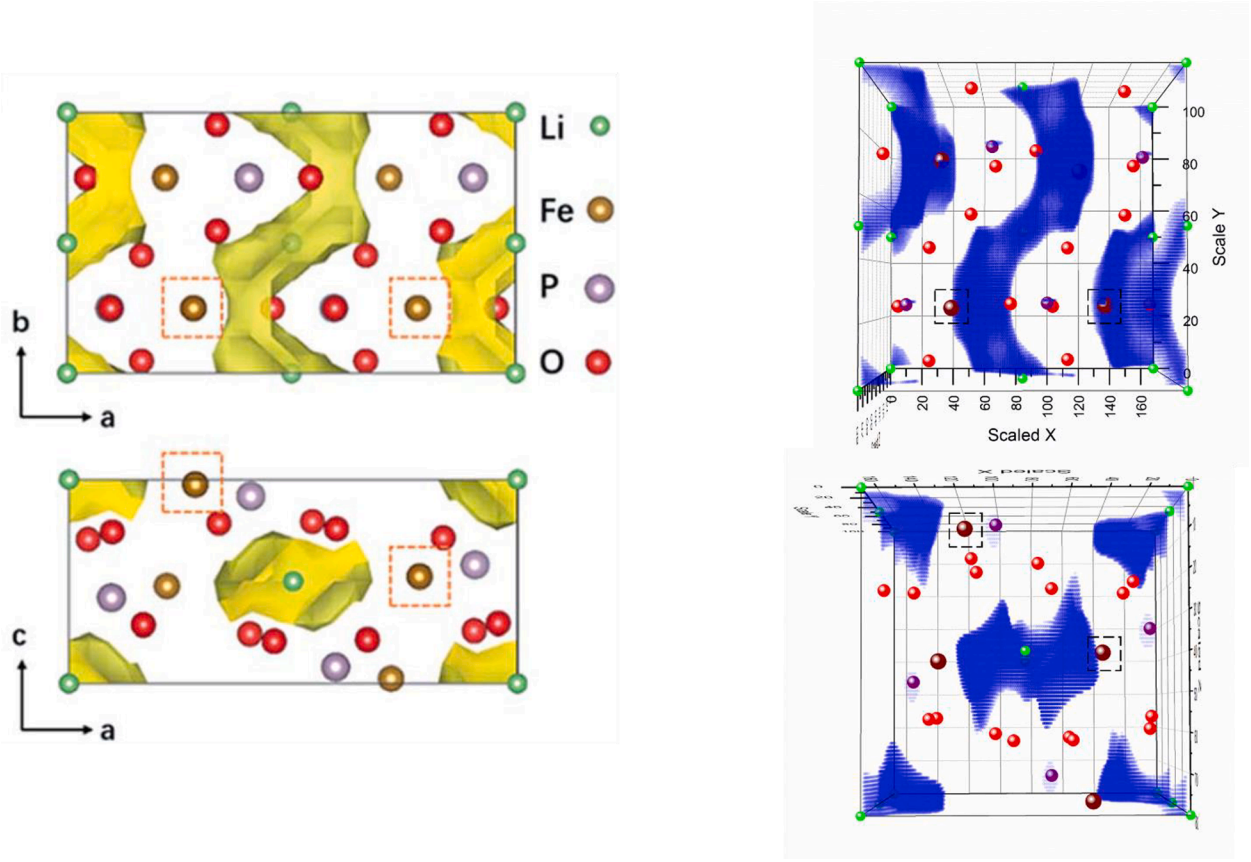

Fig. 2. The comparison pathway of $LiFePO_4$ between BV prediction by Chen's group [14] (left, yellow highlight) and our prediction (right, blue highlight). Note that we used scaled X, Y, and Z axis for all crystal structures then plot them in the cubic form.

structures, which will provide an innovative way for future large scale material screening and high-throughput calculation.

2. Model structures and computational details

Density functional theory (DFT) calculations were performed as implemented in the VASP package [17]. The PAW pseudopotentials[18] will be used to treat outermost electrons as valence electrons of atoms. The Perdew-Burke-Ernzerhof (PBE) parameterization within the generalized gradient approximation (GGA) [19] were adopted to describe the exchange and correlation functional. Integrations over the Brillouin zone were performed using Monkhorst-Pack grids. The density of *k*-point sampling in the Brillouin zone was generally taken as 0.03 $(1/\text{Å})$ for the unit cell, and the plane-wave cutoff energy was set to 500 eV. The 3D electronic charge density distribution can be outputted immediately after the atomic structure optimization. For comparison, the transport paths for Li ion in $Li_5PS_4Cl_2$ and $Li_3Y(PS_4)_2$ lattice were also calculated using the climbing-image nudged elastic band method in a $2 \times 1 \times 1$ supercell. A $2 \times 2 \times 2$ k-point grid was used and the cutoff of the kinetic energy was set to 500 eV for all climbing-image nudged elastic band method calculations. The supercells containing excess electrons were compensated with a uniform background charge.

3. Results and discussion

DFT reformulates the Schrödinger equation, which describes the behavior of electrons in a system. The solution of the Schrödinger equations leads to the concurrent energy and electronic charge density of the ground state, and in principle all quantities can be derived from them. The spatial distribution and patterns of electronic charge density is unique for each specific material, and therefore it is natural to expect that such patterns can also reflect the energy landscape in the system and thus can serve as the descriptor of Li-diffusion (mainly determined by energy barrier) in battery materials. From previous study, it has known that HOMO (the highest occupied molecular orbital) electronic state was useful to comprehensive the Li^+ diffusion process on a surface of carbon, which showed the Li^+ ion diffuses along a node of the HOMO [20]. Similar to the bond valence mismatch analysis the experimental nuclear density maps reveal a zigzag shape of the lithium diffusion pathway in LATP, occurring between two adjacent Li1 positions through a M3 (Li3) position [21]. The configuration of the ZVE (regions with zero density of valence electrons) also help us understand the difference of orientation on Li ions diffusing in c-Si [22]. In general, lithium ions are prone to migrate along the pathway/space that avoid the strong electron interaction from atom core and covalence bond and thus reduce the active energy [20–22]. The ionic conductivity of solid-state lithium electrolytes is generally determined by the ease of Li ions transport through open spaces (i.e., diffusion channels).

In order to test the accuracy of electronic charge density serve as the descriptor of Li-diffusion, we compared the visualized electronic charge density and the diffusion channels of several well-studied high Li ionic conductivity materials. The first material studied was $Li_5PS_4Cl_2$, which was recently discovered as lithium thiophosphates family crystalline superionic conductors, and the results are shown in Fig. 1. The picture in Fig. 1(a) and 1(c) shows the Li ion migration channels which were predicted by Zhu et al. [12] using FPMD simulations. The channels can be classified into three distinct types: (1) those parallel to the *b*-*c* plane and transport through *c*-axis, (2) parallel to the *b*-*c* plane and along the *b*-axis, and (3) along the *a*-axis of the unit cell. These three types of channels are referred to as $A \rightarrow B$, $B \rightarrow C$, and $A \rightarrow D$ pathways (denoted by light green spheres in Fig. 1), respectively. With the crystal symmetry of *Amm*2, all diffusion channels in the crystal are rotated and/or mirrored

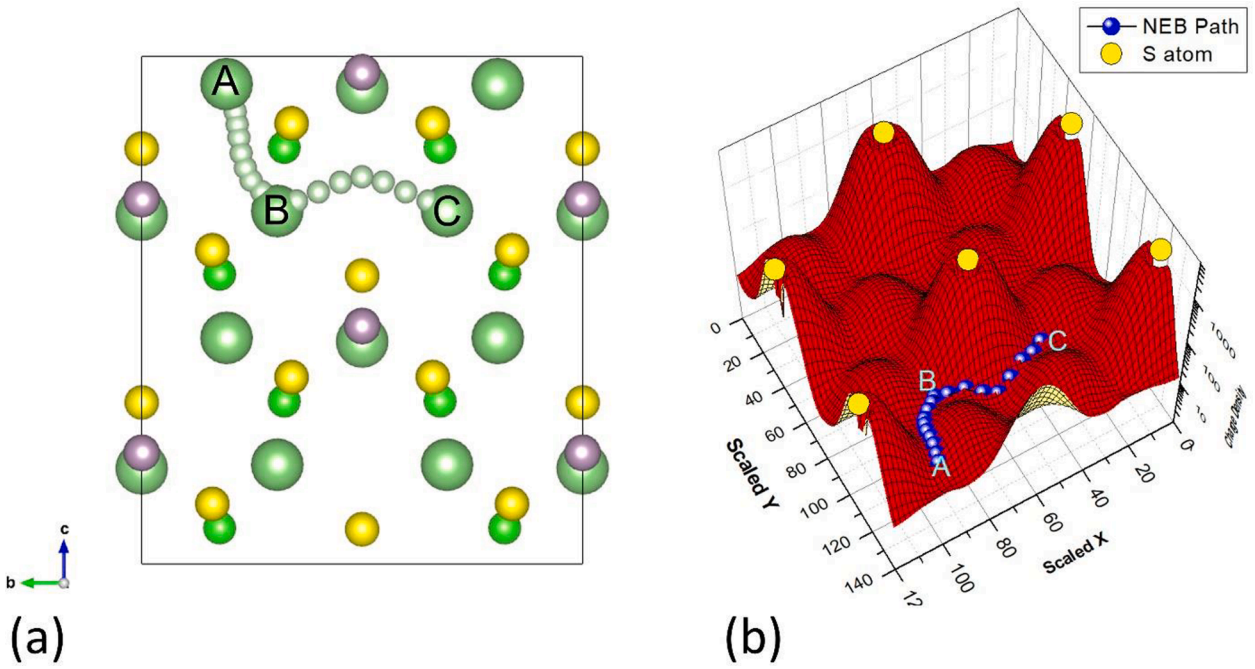

Fig. 3. Li ion transport channel in $Li_5PS_4Cl_2$. (a) Li-ion migration path predict by NEB calculation (light green balls). (b) Electronic charge density distribution in the *A-B-C* section plane as indicated in the left panel. The migration path predicted by NEB method is denoted by the blue balls.

versions of the three reference channels. Fig. 1(b) and 1(d) shows the 3D spatial electronic charge density of $Li_5PS_4Cl_2$, which is the section of electronic charge density on the *b-c* plane containing Li ion diffusion channel and the section of *ac* plane. In this picture the scaled X, scaled Y and scaled Z corresponds to a-axis, b-axis and c-axis, respectively. The dark blue points denote the lower electronic charge density region (populations) and the red arrows are replotting the migration paths from the left panel. The lighter blue point means higher charge density, and the hollow region means a spherical region around a nucleus (such as S atom) with ultra-high charge density. For $Li_5PS_4Cl_2$, these dark blue channel for Li^+ migration corresponds to regions possessing the smallest numbers of electrons. If these spaces are oriented along a direction parallel to the Li^+ concentration gradient, they can serve as preferential passages for Li^+ diffusion. Such characteristics of ionic transport permit the prediction of diffusion pathways in $Li_5PS_4Cl_2$. By comparing the previous diffusion paths from FPMD simulations [12] [shown in Fig. 1 (a) and (c)] with the electronic charge density distribution [Fig. 1(b) and (d)], it is found that the Li^+ ions diffuse along the dark blue channel of low density region and avoid the high electronic charge density from atom core in all three directions. To visualize the Li path, we calculate the gradient and the Hessian matrix of charge data to screen the valley path (Detail can be found in the Supporting information), and then we use an appropriate charge isosurface (C_{iso}) predict Li path. The value of charge density C_{iso} is a normalized parameter, which is the value of charge density divided by number of electrons. An appropriate C_{iso} should be chose to reveal the data point of valley path in picture. In the aim of comparing the visualized Li path of our method with the well-known BV method, we choose a charge isosurface $C_{iso} = 0.059$ and plot Li path of $LiFePO_4$ in Fig. 2. The Li path of $LiFePO_4$ is as agree with that predicted by Chen's group to retrieve the bottleneck of the diffusion path [14]. Moreover, our first-principles charge density figure gives more detailed information in the following discussion.

Since the most possible Li^+ migration paths in $Li_5PS_4Cl_2$ were already identified [12], we re-examined this structure and showed our NEB calculation in Figs. 3(a) and S1, i.e. the *A*→*B* path parallel to the *b-c* plane and transport through *c*-axis, and the *B*→*C* path parallel to the *b-c* plane and along the *b*-axis. In Fig. 3(b) we plot 3D spatial electronic charge density surface distribution in a section plane (parallel to the *b-c* plane) which is superimposed with probable diffusion pathways (denoted by the blue ball connecting the Li^+ sites). In this picture the scaled *X* and scaled *Y* corresponds to *b*-axis and *c*-axis, respectively, and *Z* corresponds to the charge density. Obviously, these diffusion pathways connect the Li^+ sites along the low charge density valley while evading high charge density regions around the anions such as S and P. This is understandable because the S atom interacts strongly with the Li^+ ion in diffusion pathway. In Fig. 3(b), a good agreement between NEB theory path and the valley featured with low charge density can be noticed: similar to the NEB theory prediction, the charge density valley reveals a connective pathway between adjacent Li^+ positions in $Li_5PS_4Cl_2$ by bypassing charge density peaks.

These results imply that it is possible to find Li^+ diffusion pathways directly from the 3D spatial electronic charge density distribution. Since the ionic conductivity is directly proportional to $e^{-\Delta E_a/k_BT}$ [23,24], where ΔE_a, k_B, and T are the diffusion energy barrier, Boltzmann constant, and system temperature, respectively, the ionic conductivity can be evaluated by calculating the energy barrier for Li^+ diffusion along the diffusion pathways (by determining the dominant factor ΔE_a). Since the most thermodynamically favorable energy barrier can be calculated in NEB simulation, we can also obtain the corresponding energy barrier from an estimated NEB path in Fig. 3(b). By using NEB calculation coupled with first-principles, the reference [12] predicted Li^+ ion migration energy barrier of path *A*→*B* as 0.168 eV and the energy barrier of path *B*→*C* as 0.271 eV, respectively. The predicting energy barrier along the *A*→*B* and *B*→*C* valley pathway are 0.301 eV and 0.209 eV, respectively. Our predicted energy barriers are in reasonable agreement with the accurate NEB calculations. In addition, energy barrier calculation also gives a restrict to predicted charge isosurface C_{iso}, which lead to the appropriate C_{iso} be smaller to elimate the data point with high energy for these Li ionic conductivity materials. It is worth pointing out that, the difference between our model and the NEB calculation might be attributed to the frozen charge density induced migration paths deviation. The average sampling points used for electronic charge density method is surely another origin for the difference. However, we can quickly find out the possible pathway with small energy barriers, then we can still further check the energy barrier of these candidate paths by NEB method.

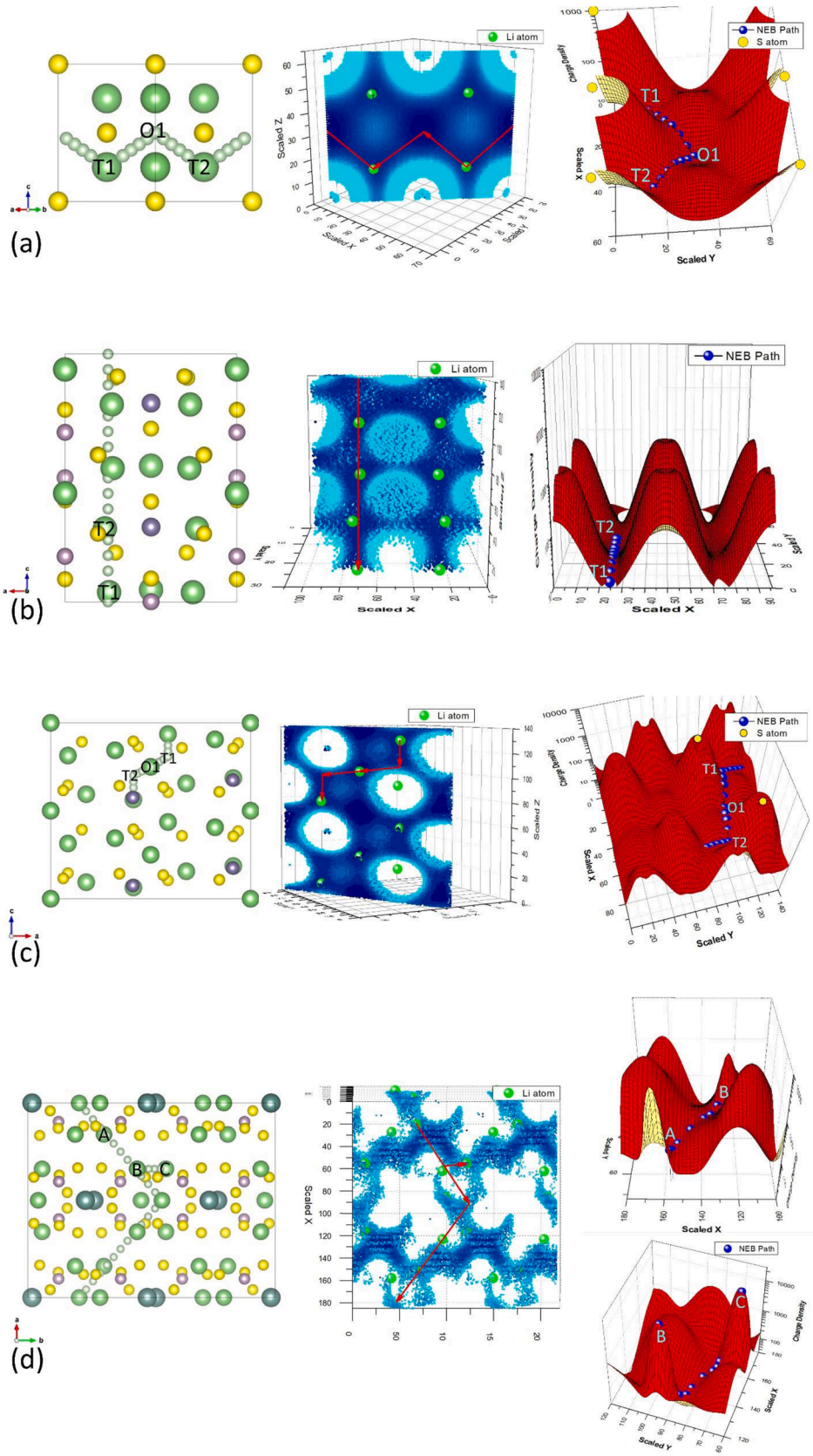

Fig. 4. Li ion transport in some representative superionic conductors: (a) Li_2S, (b) $Li_{10}GeP_2S_{12}$, (c) Li_4GeS_4, and (d) $Li_3Y(PS_4)_2$. (Left panel) Li-ion migration path predict by NEB calculation (light green balls). (Middle panel) Spatial distribution of electronic charge density. The lithium ions are shown by the green balls and the dark blue region represents the possible Li ion diffusion channel. The red arrows indicate the migration channels from the left panel. (Right panel) Electronic charge density prediction along selected plane as labeled in the left panel. The migration path predicted by NEB method is denoted by the blue balls.

We further performed calculations for several other well-known lithium-containing solid electrolyte materials, namely Li_2S, $Li_{10}GeP_2S_{12}$, Li_4GeS_4 and $YLi_3(PS_4)_2$, with their electronic charge density shown in Fig. 4, and their Li^+ diffusion pathways predicted by Zhu et al. using FPMD simulations [12] are plotted by the light green balls as well as the red arrows in Fig. 4. These systems were selected due to the available comprehensive DFT calculation on the mechanism of high ionic conductivity [11,12]. In the study of Wang et al. [11], the Li_2S, $Li_{10}GeP_2S_{12}$ and Li_4GeS_4 have simple diffusion pathways which are similar as that in face-centered cubic (fcc), body-centered cubic(bcc), and hexagonal close-packed (hcp) lattices, respectively. For example, Fig. 4(a) shows the case of Li_2S structure (left panel) with diffusion channel (light green balls). In the fcc anion lattice, the Li^+ migration between two tetrahedral sites [labeled as "T1" and "T2" in Fig. 4(a)] is through an intermediate octahedral site (labeled as "O1"), hereafter denoted as the "T-O-T" path. While the middle panel in Fig. 4 shows the electronic charge density with the possible diffusion channel, and the right panel shows the landscape of charge density with NEB path. For Li_2S, as presented in the FPMD simulation [11], the Li^+ ion vibrates in the pocket of site T1 or T2. The Li^+ ion can hardly escape from the edge site at 300 K. Fig. 4(b), (c), and (d) corresponds to the case of $Li_{10}GeP_2S_{12}$, Li_4GeS_4 and $YLi_3(PS_4)_2$, respectively. In the bcc liked $Li_{10}GeP_2S_{12}$ lattice, the Li^+ ion migrates with a remarkably low barrier along a path connecting two face-sharing tetrahedral sites [labeled as "T1" and "T2" in Fig. 4(b)] [11]. In the hcp liked Li_4GeS_4 lattice, the T-O-T type path can be also found in the *a-c* plane of the hcp lattice ["T1" to "T2" through "O1" in Fig. 4(c)] [11]. We re-examined the $YLi_3(PS_4)_2$ structure and showed our NEB calculation in Fig. 4(d). Once again, all these results unambiguously demonstrate that the Li^+ ions tend to migrate along the valleys of local electronic charge density regions, corresponding to low electronic charge densities, while trying to avoid the high electronic charge density regions. The valleys of the landscape of the spatial charge densities clearly point out the migration pathways of Li ions. The electronic charge density method reproduces these paths perfectly predicted by FPMD simulations as well as by the NEB calculations. This proves that the results of our method are correct and demonstrates a major success of our electronic charge density method.

4. Conclusion

In summary, we proposed a spatial electronic charge density method to simulate Li-diffusion pathways for solid-electrolyte materials, which can be outputted simultaneously from first-principles structure optimization. This new method has low computational cost as compared to the traditionally widely used methods, such as FPMD and NEB, and in the meantime maintains high precision for finding Li-ion migration pathways. We validated our method by studying several complex electrolyte materials with high ionic conductivity [$Li_5PS_4Cl_2$, $Li_{10}GeP_2S_{12}$, Li_4GeS_4, and $Li_3Y(PS_4)_2$] and one simple electrolyte structure (Li_2S), by comparing their diffusion pathways of Li^+ ions with those obtained by NEB and FPMD simulations. The Li^+ diffusion pathways predicted by our spatial electronic charge density approach are in excellent agreement with those reported in literature, confirming that our approach correctly captures the unique features of spatial energy landscapes. Since the spatial electronic charge densities are fast to calculate, we believe that this new method can dramatically speed up high-throughput structure screening for new solid electrolyte discovery in the future, in particular when combining with quantitative energy barrier calculation such as DFT, and can also serve as a new material fingerprint in material informatics and data science such as machine learning. This approach can be extended to other material fields as well, such as predicting mechanical, thermodynamic, and chemical properties.

5. Data Availability Statement

The data that support the findings of this study are available from the corresponding author upon reasonable request.

CRediT authorship contribution statement

Yinqiao Liu: Data curation, Formal analysis, Methodology, Visualization, Writing - original draft, Writing - review & editing. **Xue Jiang:** Formal analysis, Resources, Writing - review & editing, Funding acquisition. **Jijun Zhao:** Formal analysis, Resources, Writing - review & editing, Funding acquisition. **Ming Hu:** Conceptualization, Formal analysis, Methodology, Resources, Supervision, Visualization, Writing - original draft, Writing - review & editing, Funding acquisition.

Declaration of Competing Interest

The authors declare that they have no known competing financial interests or personal relationships that could have appeared to influence the work reported in this paper.

Acknowledgements

Research reported in this publication was supported in part by the NSF (award number 2030128, 1905775) and SC EPSCoR/IDeA Program under NSF OIA-1655740 via SC EPSCoR/IDeA 20-SA05. The views, perspective, and content do not necessarily represent the official views of the SC EPSCoR/IDeA Program nor those of the NSF. This work was also supported by the National Natural Science Foundation of China (11874097) and the Fundamental Research Funds for the Central Universities of China (DUT19LK12).

Appendix A. Supplementary data

Supplementary data to this article can be found online at https://doi.org/10.1016/j.commatsci.2021.110380.

References

[1] J.M. Tarascon, M. Armand, Issues and challenges facing rechargeable lithium batteries, in: Materials for Sustainable Energy, Co-Published with Macmillan Publishers Ltd, UK, 2010, pp. 171-179.
[2] E. Karden, S. Ploumen, B. Fricke, T. Miller, K. Snyder, J. Power Sources 168 (2007) 2–11.
[3] J.B. Goodenough, Y. Kim, Chem. Mater. 22 (2010) 587–603.
[4] K. Takada, Acta Mater. 61 (2013) 759–770.
[5] K. Xu, Chem. Rev. 104 (2004) 4303–4418.
[6] M. Yashima, M. Itoh, Y. Inaguma, Y. Morii, J. Am. Chem. Soc. 127 (2005) 3491–3495.
[7] J. Han, J. Zhu, Y. Li, X. Yu, S. Wang, G. Wu, H. Xie, S.C. Vogel, F. Izumi, K. Momma, Y. Kawamura, Y. Huang, J.B. Goodenough, Y. Zhao, Chem. Commun. 48 (2012) 9840–9842.
[8] C.A. Geiger, E. Alekseev, B. Lazic, M. Fisch, T. Armbruster, R. Langner, M. Fechtelkord, N. Kim, T. Pettke, W. Weppner, lnorg, Chem. 50 (2011) 1089–1097.
[9] W. Li, G. Wu, C.M. Araújo, R.H. Scheicher, A. Blomqvist, R. Ahuja, Z. Xiong, Y. Feng, P. Chen, Energy Environ. Sci. 3 (2010) 1524–1530.
[10] S. Adams, R.P. Rao, J. Mater. Chem. 22 (2012) 1426–1434.
[11] Y. Wang, W.D. Richards, S.P. Ong, L.J. Miara, J.C. Kim, Y. Mo, G. Ceder, Nat. Mater. 14 (2015) 1026.
[12] Z. Zhu, I.-H. Chu, S.P. Ong, Chem. Mater. 29 (2017) 2474–2484.
[13] N.A. Katcho, J. Carrete, M. Reynaud, G. Rousse, M. Casas-Cabanas, N. Mingo, J. Rodriguez-Carvajal, J. Carrasco, J. Appl. Crystallogr. 52 (2019) 148–157.
[14] D. Chen, J. Jie, M. Weng, S. Li, D. Chen, F. Pan, L.-W. Wang, J. Mater. Chem. A 7 (2019) 1300–1306.
[15] S. Adams, R.P. Rao, physica status solidi (a) 208 (2011) 1746–1753.
[16] S. Adams, R.P. Rao, Understanding Ionic Conduction and Energy Storage Materials with Bond-Valence-Based Methods, in: I.D. Brown, K.R. Poeppelmeier (Eds.), Bond Valences, Springer, Berlin Heidelberg, Berlin, Heidelberg, 2014, pp. 129–159.
[17] G. Kresse, J. Furthmüller, Phys. Rev. B 54 (1996) 11169–11186.
[18] P.E. Blöchl, Phys. Rev. B 50 (1994) 17953–17979.
[19] J.P. Perdew, K. Burke, M. Ernzerhof, Phys. Rev. Lett. 77 (1996) 3865–3868.
[20] H. Tachikawa, A. Shimizu, J. Phys. Chem. B 109 (2005) 13255–13262.

[21] M. Monchak, T. Hupfer, A. Senyshyn, H. Boysen, D. Chernyshov, T. Hansen, K. G. Schell, E.C. Bucharsky, M.J. Hoffmann, H. Ehrenberg, lnorg, Chem. 55 (2016) 2941–2945.
[22] Y.-S. Choi, J.-H. Park, J.-P. Ahn, J.-C. Lee, Sci. Rep. 7 (2017) 14028.
[23] X. He, Y. Zhu, Y. Mo, Nat. Commun. 8 (2017) 15893.
[24] P.n. Huang, A. Petric,, J. Electrochem. Soc. 143 (1996) 1644–1648.